2018

Effects of resonant-laser excitation on the emission properties in a single quantum dot

O. Gazzano
National Institute of Standards and Technology and University of Maryland

T. Huber
National Institute of Standards and Technology and University of Maryland

V. Loo
National Institute of Standards and Technology and University of Maryland

S. Polyakov
National Institute of Standards and Technology

E.B. Flagg
West Virginia University

See next page for additional authors

Research Article Vol. 5, No. 4 / April 2018 / Optica 354

Effects of resonant-laser excitation on the emission properties in a single quantum dot

O. Gazzano,[1] T. Huber,[1] V. Loo,[1] S. Polyakov,[2] E. B. Flagg,[3] and G. S. Solomon[1,2,*]

[1]Joint Quantum Institute, National Institute of Standards and Technology and University of Maryland, College Park, Maryland 20742, USA
[2]National Institute of Standards and Technology, Gaithersburg, Maryland 20899, USA
[3]Department of Physics and Astronomy, West Virginia University, Morgantown, West Virginia 26506-6315, USA
*Corresponding author: gsolomon@umd.edu

Received 28 November 2017; revised 21 January 2018; accepted 23 January 2018 (Doc. ID 314469); published 27 March 2018

While many solid-state emitters can be optically excited non-resonantly, resonant excitation is necessary for many quantum information protocols as it often maximizes the non-classicality of the emitted light. Here, we study the resonance fluorescence in a solid-state system—a quantum dot—with the addition of weak, non-resonant light. In the inelastic scattering regime, changes in the resonance fluorescence intensity and linewidth are linked to both the non-resonant and resonant laser powers. Details of the intensity change indicate that charge-carrier loss from the quantum dot is resonant laser. As we enter the Mollow triplet regime, this resonant laser loss term rate is approximately $1/50\ \mathrm{ns}^{-1}$. This work further clarifies resonance fluorescence in solid-state systems and will aid in the further improvement of solid-state non-classical light sources.

OCIS codes: (300.6280) Spectroscopy, fluorescence and luminescence; (250.5590) Quantum-well, -wire and -dot devices.

https://doi.org/10.1364/OPTICA.5.000354

1. INTRODUCTION

Ideally, the light spontaneously emitted by an isolated two-level system has a Lorentzian line shape representing the Fourier transformation of the spontaneous emission process. The spectral linewidth γ is then determined by only the dipole radiative decay rate Γ by the relation $\gamma = \Gamma/2$. A real world solid-state emitter, however, interacts with its environment. With environmental coupling, the emitter spectrum can be broadened, and its line shape will be modified depending on the characteristic time and interaction rate of the coupling. Fast coupling mechanisms, on the timescale of Γ^{-1}, homogeneously broaden the Lorentzian line shape spectrum so that $\gamma = \Gamma/2 + \gamma^{\star}$, where $\gamma^{\star}$ is the pure dephasing rate. Slow environmental coupling induces spectral wandering and leads to an inhomogeneous component in the line shape. These broadening processes reduce the emitted photon indistinguishability.

For many quantum information and quantum optics applications [1–5], resonant excitation is important as it eliminates the time uncertainty in the state preparation [6–8] and increases photon indistinguishability. Resonant excitation of a solid-state quantum emitter can transfer the laser coherence to the excited state. This can be used, for instance, to generate time-bin entangled photon pairs, where the phase of the laser is transferred to the photons [9]. In some solid-state systems, the quality of spin state preparation and readout can also be improved [10].

Semiconductor quantum dots (QDs) of InAs embedded in a solid-state host are bright emitters of single and indistinguishable photons and are good candidates for applications in quantum information [11–13]. Better quantum properties of the photons have been observed under resonant excitation [14–17]. However, in QD resonant excitation, the fluorescence is often strongly reduced compared to the non-resonant case and remains spectrally broad, limiting the scope of applications [18,19]. Furthermore, the photon indistinguishability drops for photons emitted temporally more than a few hundreds of nanoseconds apart [20–22]. Thus, for a variety of quantum information processes using QDs—for instance, entanglement distribution [2,23], photon multiplexing [21,24], or multiple sources experiments [25,26]—resonance fluorescence and the long time scale energy fluctuations in quantum dots must be better understood.

In this paper, we study the effects of a resonant-laser excitation in a QD, using a weak above-band laser as a probe in conjunction with the resonance fluorescence. The additional pump produces no measurable photons in the region of interest when the resonant laser is switched off, but provides charge carriers to the system. First, we show that light from a weak above-band laser can improve the brightness of a resonantly pumped QD transition by a factor larger than 30 and reduces its inhomogeneous transition linewidth by a factor of about 2. The brightness improvement has been previously reported [18,19,27], but to our knowledge, the linewidth narrowing has not. Second, we show using both experimental data and Monte Carlo simulations that a carrier loss term that depends on the resonant laser power is present and to our knowledge has not been previously discussed. This resonant

laser-induced loss could have implications for other solid-state systems beside QDs.

2. EXPERIMENTS

The sample was made by molecular-beam epitaxy. It consists of strain-induced InAs QDs in GaAs embedded in a $4\lambda/n$ thick planar distributed Bragg reflector cavity (λ is the cavity resonance wavelength, and n is the GaAs refractive index). The cavity enhances the fluorescence collection through the upper sample surface, resulting in extraction efficiencies of 10% to 20% [28]. We observe a single charged exciton and show that the observed emission under resonant excitation has a low multi-photon contribution: $g^{(2)}(0) = 0.22 \pm 0.03$ (no dark count or background subtraction). From the data, we determine the radiative decay rate, $\Gamma = 1.5\ \mathrm{ns}^{-1}$, and thus a radiative-limited linewidth of 250 MHz.

To suppress the resonant laser scattering from the QD fluorescence signal, we use an orthogonal excitation-collection scheme: the excitation laser light is fiber-coupled to the side of the sample and propagates in-plane, and the collection axis is normal to the plane (Fig. 1) [29,30]. The in-plane pump laser couples predominantly to the $4\lambda/n$ cavity region, which forms an in-plane waveguide. The QD emission is collected vertically with a high-numerical-aperture objective and is coupled into a single-mode fiber.

The resonant light source is a tunable continuous-wave (CW) laser (200 kHz linewidth). Its frequency is measured using a wavelength meter. The weak above-band light is a 633 nm HeNe laser and is sent to the sample surface through the collection optical fiber (Fig. 1). Polarizers and polarization controllers inserted in the excitation laser path and collection path further minimize the detected laser scattering. The sample is cooled to 4.2 K using a helium bath cryostat.

As has been previously reported [18,19], the on-resonance fluorescence signal is weak for most QD states, and weak above-band light can enhance the fluorescence intensity. We measure large photon intensity improvements for many QDs, but not for all of them. For all the results of this study, the power of the HeNe laser beam on the sample is on the order of nanowatts, and no photoluminescence signal from the HeNe alone is measured. Measurements were made at a variety of Rabi frequencies varying from near zero to 0.7 GHz.

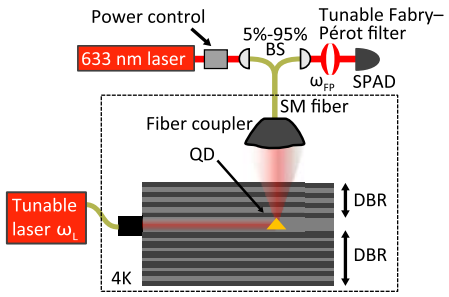

Fig. 1. Schematic of the experiment. A single-mode (SM) optical fiber is glued to the cleaved edge of the sample to resonantly excite a QD embedded between two distributed Bragg reflectors (DBR). The light is collected from the sample top surface using a fiber-coupled microscope objective. The weak, 633 nm laser is sent to the sample using the same objective. The Fabry–Pérot filter is bypassed in the resonance fluorescence spectroscopy scans. BS: beam splitter; SPAD: single photon avalanche photodiode.

3. RESONANCE FLUORESCENCE MAPS

To investigate the effects of broadening mechanisms on the emission properties from exciton transitions in resonant excitation, we measure resonance fluorescence maps in the elastic scattering regime. Such maps represent the QD fluorescence intensity I_{Exp} as a function of both the pump laser frequency ω_L and the fluorescence frequency ω_{Ph}. To do this, we use the tunable CW laser and a 200 MHz band-pass Fabry–Pérot filter (Fig. 1). We obtain a map through a series of resonance fluorescence spectroscopy scans (i.e., by scanning the Fabry–Pérot filter frequency) for several laser frequencies. An identical map could also be obtained by scanning the laser frequency and keeping the filter position constant for each scan. We measure the QD fluorescence intensity for each point using a single-photon avalanche photodiode connected to an event-counting module.

We use the detuning-dependent resonance fluorescence equations of a coherently driven two-level system [31,32] to calculate fluorescence maps. Results in the inelastic scattering regimes are plotted and discussed in Supplement 1. We discuss here the elastic scattering regime (also called the Rayleigh scattering regime). In the ideal case (narrow linewidth laser, Fabry–Pérot filter, and QD state), the map is a point centered on the QD state frequency. For a real-world case, this ideal response is successively convolved by the laser line shape (convolved along the ω_L axis), the detector response (convolved along the ω_{Ph} axis), and the QD state broadening (convolved along the diagonal direction, $\omega_{\mathrm{ph}} = \omega_L$). The QD state broadening is Gaussian in the case of inhomogeneous broadening and Lorentzian in the case of

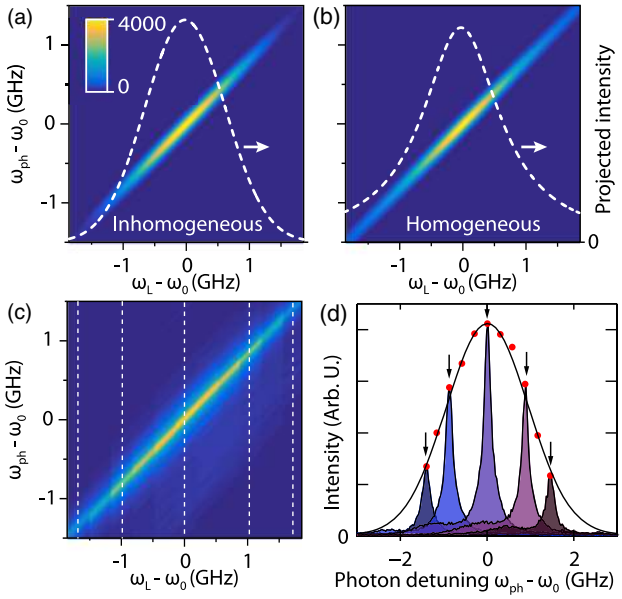

Fig. 2. Characterizing the linewidth. (a), (b) Theoretical fluorescence maps of emission from a QD transition with (a) inhomogeneous or (b) homogeneous broadening. The shape of the intensity distribution in the diagonal $\omega_{\mathrm{ph}} = \omega_L$ is Gaussian in the inhomogeneous case and Lorentzian in the homogeneous case, as indicated by the white dotted lines. (c) Experimental fluorescence map obtained by sweeping the frequency of a laser ω_L and of a Fabry–Pérot filter ω_{ph} around the QD frequency, ω_0. (d) Shaded curves: resonance fluorescence spectra obtained for different laser frequencies, as indicated by dotted lines in (c). The red dots indicate the resonance fluorescence maximum for each laser frequency. The envelope intensity is Gaussian (black line).

homogeneous broadening [33]. Thus, one can distinguish between inhomogeneous and homogeneous broadening by evaluating the diagonal lineshape. Calculated maps are plotted in Figs. 2(a) and 2(b).

A measured fluorescence map $I_{\mathrm{Exp}}(\omega_{\mathrm{Ph}}, \omega_L)$ is shown in Fig. 2(c) in the elastic scattering regime with the additional HeNe laser (≈20 nW). We observe that the fluorescence map has an oval-like shape strongly elongated along the $\omega_L = \omega_{\mathrm{Ph}}$ diagonal. From this fluorescence map, we take resonance fluorescence spectra for specific values of ω_L [vertical dotted lines in Fig. 2(c)]. Example resonance fluorescence spectra are plotted in Fig. 2(d) for these laser frequencies. Each spectrum has 200 MHz Lorentzian line shape, which is determined by a convolution of the laser line and the Fabry–Pérot interferometer response. Red dots in Fig. 2(d) represent the resonance fluorescence peak intensity for different laser frequencies in the fluorescence map. Here, the intensity of the spectra corresponds to the probability of overlap of the broadened QD transition frequency with the laser frequency. We observe that the intensity of the resonance fluorescence spectrum as a function of the laser detuning is fit by a Gaussian distribution function (solid black line) and thus deduce that the broadening is inhomogeneous. This means that the QD transition energy is not constant in time but varies. We previously reported an energy jitter timescale of ≈24 ns with a similar sample by using second-order autocorrelation measurements [34]. We measure here that the full width at half-maximum of the Gaussian distribution of the emission is ≈2.5 GHz in Fig. 2(d). The small feature on the low-energy side of the resonance peak is likely to due to the Fabry–Pérot filter.

4. ENHANCED INTENSITY AND RESONANT-LASER-INDUCED LOSS

In this section, we investigate the effects of carrier population dynamics on the resonance fluorescence in the inelastic scattering regime with the addition of above-band light of variable intensity. Because we have established that the broadening is predominantly inhomogeneous, we no longer need to scan the detection wavelength as in the resonance fluorescence maps above. In each spectrum, we sweep the CW laser through the QD transition and count detected QD photons as a function of the laser frequency. Since the remaining Lorentzian component is due to the radiative lifetime and power broadening induced by the laser, the resonance fluorescence spectrum line shape is the convolution of the Lorentzian and the Gaussian broadening components of the QD emission, a Voigt function. The full width at half-maximum of the Lorentzian is determined by the relation $\sqrt{T_1^{-2} + 2\Omega_r^2}$, where Ω_r is the Rabi frequency [35]. Ω_r^2 is proportional to the laser power and is determined using CW second-order autocorrelations on the QD photons [35], shown in Fig. 3(a). We fit the resonance fluorescence spectra using a Voigt function to extract the amplitude and the linewidth of the Gaussian component.

We plot in Fig. 3(b) the integrated resonance fluorescence spectra intensity as a function of the HeNe laser power. The data show that adding the above-band laser initially increases the resonance fluorescence-integrated intensity. The peak intensity also increases, as shown in Fig. 3(c) and in more detail in Supplement 1. The maximum peak intensity increases by a factor ≈30 and the integrated intensity by a factor ≈17, as illustrated in Fig. 3(c). Figure 3(b) also shows that the peak brightness is retarded with the HeNe power as the resonance fluorescence power increases [black crosses in Fig. 3(b)]. This is discussed in more detail below.

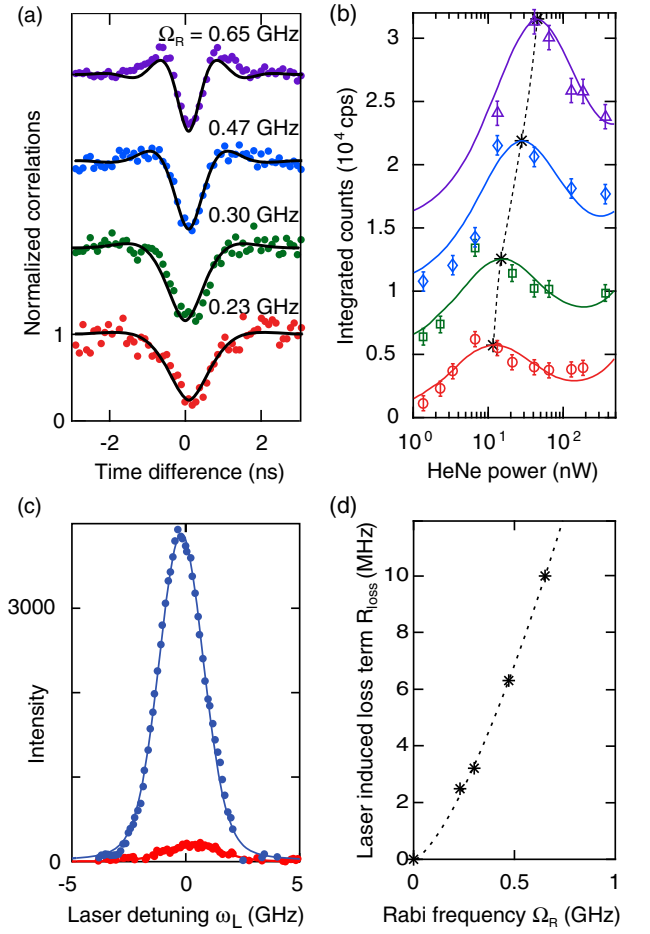

Fig. 3. Enhanced intensity and resonant-laser induced loss. (a) Autocorrelation measurements performed under CW resonant excitation and for different Rabi frequencies (i.e., resonant laser powers). (b) Integrated intensity as a function of HeNe power and for several resonant laser powers (red circles: $\Omega_r = 0.23$ GHz, green squares: $\Omega_r = 0.30$ GHz, blue diamonds: $\Omega_r = 0.47$ GHz, violet triangles: $\Omega_r = 0.65$ GHz). The solid lines represent the simulation; see text for details. The data with $\Omega_r = 0.47$ GHz (blue diamonds) has an increase of integrated brightness of 17 with respect to its lowest value. The four curves were offset by 5000 counts each for clarity. The HeNe spot size is approximately 1 μm in diameter. (c) Resonance fluorescence excitation spectroscopy of a QD transition for two above-band 633 nm laser powers (red dots: 1.3 nW; blue dots: 40 nW). The intensity is not normalized to show the strong brightness improvement by a factor of 30. (d) Plot of the resonant-laser-induced loss term, obtained by fitting the data with the Monte Carlo simulation, as a function of the Rabi frequency Ω_R.

To gain more insight into the dynamics of the resonant excitation with additional HeNe laser, we programmed a Monte Carlo simulation to model the emission dynamics. The model is based on probabilities of events occurring in a single particle picture. It considers separate electron (e^-) and hole (h^+) empty and occupied ground states, with fermion statistics. A higher excited state for each carrier type (with infinite occupation) can also be populated (see Supplement 1).

We simulate all the experiments with a negatively charged exciton as the resonant state and a single parameter set, taking only the five most crucial parameters into account. They are coherent resonant scattering of photons on a trion transition if a single e^- ground state (of either spin) is present, creation and capture of charges generated by the above-band light source, non-radiative relaxation from the excited state to the ground state, radiative decay of bright exciton states for which only the negatively charged ground-state exciton decay contributes to observed intensity, and a resonant-laser-induced charge-carrier loss term. The model could consider radiative decay from the excited state, asymmetric capture of carriers, spin flip of charges, and loss of charges only from the excited level, but those parameters are not relevant to fit the experimental data. The results of the simulation are plotted with solid lines in Fig. 3(b) and the values of the parameters that we consider are in Table S1 of Supplement 1. The parameters are simultaneously fit for all four Rabi frequencies. The error (≈5%) is determined from repeated measurements.

The Monte Carlo simulations show that because of the presence of loss, if additional carriers are provided to the QD by the above-band light, the time the QD spends in the desired exciton state can be extended, increasing the photon flux. However, if the above-band light creates too many charges, the total amount of emitted photons will decrease again [Fig. 3(b)]. Experimentally, the photoluminescence signal created directly by the HeNe laser is seen for powers larger than $\approx 10^3$ nW.

The shift of the maximum of intensity when the resonant laser power increases [black crosses in Fig. 3(b)] is due to charge loss that depends on the resonant-laser power. To reestablish the proper carrier configuration in the quantum dot additional carriers are needed, and these carriers are provided by the above-band light source. The values of the resonant-laser-induced charge loss rate are plotted in Fig. 3(d). As we enter the Mollow triplet regime [$\Omega_R = 0.65$ GHz, Fig. 3(a)], the resonant laser loss term rate is approximately 10 MHz.

The Monte Carlo simulations show that the resonant laser affects the carrier population inside the QD. Neutralizing this loss with carriers from the above-band laser increases the resonance fluorescence. Voltage-biased devices (i.e., with no current flow) have been used in several QD experiments [36,37], and have been recently used in QD single-photon sources [16,38]. While these structures should aid in stabilizing the local charge environment around the QD [39], they may not neutralize the resonant-laser-induced loss from the QD [40,41].

5. LINEWIDTH NARROWING

Using the resonance fluorescence fits described above, we now plot in Fig. 4(a) the inhomogeneous linewidth as a function of the HeNe power and for several resonant laser powers. We observe the Gaussian linewidth is reduced by a factor of ≈2 [as illustrated in Fig. 4(b)]. An exponential dependent change in the inhomogeneous exciton emission linewidth with above-band laser power is observed for over two decades of laser power in Fig. 4(a). The measured linewidth as a function of the HeNe laser power P_{HeNe} is fitted in Fig. 4(a) by $(\Delta\omega_0 - \Delta\omega_1)e^{-P_{\mathrm{HeNe}}/P_0} + \Delta\omega_1$, where $\Delta\omega_0$ is the linewidth without the above-band laser, and $\Delta\omega_1$ is the linewidth for a large HeNe laser power. Two processes associated with additional carriers in the vicinity of the QD could explain the linewidth change. Screening of fluctuating charges and trap states with the addition of charge carriers can result

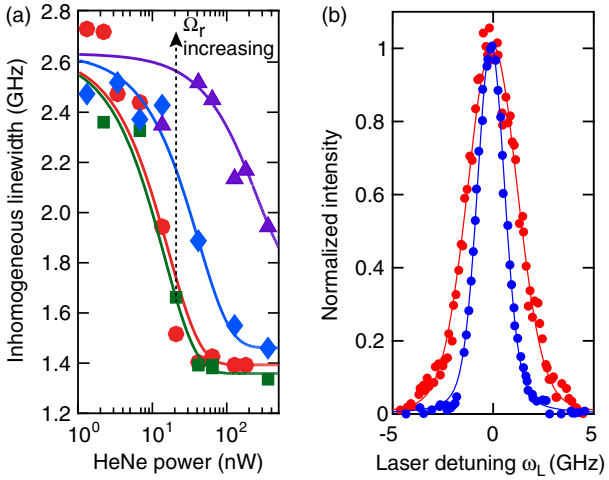

Fig. 4. Inhomogeneous linewidth narrowing. (a) Inhomogeneous linewidth of the resonance fluorescence spectra as a function of HeNe power for several resonant laser powers (red circles: $\Omega_r = 0.23$ GHz, green squares: $\Omega_r = 0.30$ GHz, blue diamonds: $\Omega_r = 0.47$ GHz, violet triangles: $\Omega_r = 0.65$ GHz). The QD inhomogeneous linewidth decreases with increased HeNe power. The decrease is slower for higher resonant laser powers. The solid lines represent exponential fits. (b) Resonance fluorescence spectrum of a QD transition for two above-band 633 nm laser powers (red dots: 1.3 nW; blue dots: 100 nW). The intensity is normalized to show the inhomogeneous linewidth narrowing.

in motional narrowing [42,43] and will be exponential in carrier population. Such traps could be local wetting layer fluctuations, nearby QD states, or defects [37]. Alternatively, stabilizing [44], as opposed to screening, fluctuating traps populations with additional carriers will have a Poissonian cumulative distribution function with a similar dependence.

Figure 4(a) shows that the linewidth narrowing is also a function of the resonant laser power. For each resonant laser power, the linewidth narrows with increased HeNe power. For higher resonant laser power, the linewidth narrowing requires stronger HeNe powers. The linewidth reaches a minimum of ≈1.4 GHz above the power-broadened radiative linewidth limit (≈0.44 GHz at $\Omega_r = 0.23$ GHz and ≈0.9 GHz at $\Omega_r = 0.65$ GHz).

In conclusion, we have experimentally investigated the radiative fluorescence from single QD states under resonant excitation. To study these effects we have introduced fluorescence maps produced by varying the detection frequency in subsequent resonance fluorescence scans near the emission resonance. This method can be used to distinguish homogeneous and inhomogeneous broadening mechanisms in solid-state two-level systems. Using a weak above-band light to provide charge carriers to the quantum dot, the QD peak emission increases by over 30 times, where the integrated intensity increases 17 times. Simultaneously, the inhomogeneous emission linewidth decreases by a factor of about 2. The change in total integrated intensity is well modeled by a simple Monte Carlo simulation where a loss term that depends on the resonant laser power must be included to replicate the observed shift in the brightness maximum with the resonant laser power. This resonant laser loss term could have implications in quantum information applications and may be present in other solid-state systems.

Funding. Physics Frontier Center at the Joint Quantum Institute (PFC@JQI).

See Supplement 1 for supporting content.

REFERENCES

1. Y. H. Shih and C. O. Alley, "New type of Einstein-Podolsky-Rosen-Bohm experiment using pairs of light quanta produced by optical parametric down conversion," Phys. Rev. Lett. **61**, 2921–2924 (1988).
2. J. I. Cirac, P. Zoller, H. J. Kimble, and H. Mabuchi, "Quantum state transfer and entanglement distribution among distant nodes in a quantum network," Phys. Rev. Lett. **78**, 3221–3224 (1997).
3. E. Knill, R. Laflamme, and G. J. Milburn, "A scheme for efficient quantum computation with linear optics," Nature **409**, 46–52 (2001).
4. M. A. Broome, A. Fedrizzi, S. Rahimi-Keshari, J. Dove, S. Aaronson, T. C. Ralph, and A. G. White, "Photonic Boson sampling in a tunable circuit," Science **339**, 794–798 (2013).
5. J. Carolan, C. Harrold, C. Sparrow, E. Martin-Lopez, N. J. Russell, J. W. Silverstone, P. J. Shadbolt, N. Matsuda, M. Oguma, M. Itoh, G. D. Marshall, M. G. Thompson, J. C. F. Matthews, T. Hashimoto, J. L. O'Brien, and A. Laing, "Universal linear optics," Science **349**, 711–716 (2015).
6. A. Kiraz, M. Atatüre, and A. Imamoğlu, "Quantum-dot single-photon sources: prospects for applications in linear optics quantum-information processing," Phys. Rev. A **69**, 1–10 (2004).
7. E. B. Flagg, S. V. Polyakov, T. Thomay, and G. S. Solomon, "Dynamics of nonclassical light from a single solid-state quantum emitter," Phys. Rev. Lett. **109**, 163601 (2012).
8. T. Huber, A. Predojević, G. S. Solomon, and G. Weihs, "Effects of photoneutralization on the emission properties of quantum dots," Opt. Express **24**, 21794–21801 (2016).
9. H. Jayakumar, A. Predojević, T. Kauten, T. Huber, G. S. Solomon, and G. Weihs, "Time-bin entangled photons from a quantum dot," Nat. Commun. **5**, 4251 (2014).
10. L. Robledo, L. Childress, H. Bernien, B. Hensen, P. F. A. Alkemade, and R. Hanson, "High-fidelity projective read-out of a solid-state spin quantum register," Nature **477**, 574–578 (2011).
11. O. Gazzano, S. Michaelis de Vasconcellos, C. Arnold, A. Nowak, E. Galopin, I. Sagnes, L. Lanco, A. Lemaître, and P. Senellart, "Bright solid-state sources of indistinguishable single photons," Nat. Commun. **4**, 1425 (2013).
12. O. Gazzano and G. S. Solomon, "Toward optical quantum information processing with quantum dots coupled to microstructures [Invited]," J. Opt. Soc. Am. B **33**, C160–C175 (2016).
13. P. Senellart, G. Solomon, and A. White, "High-performance semiconductor quantum-dot single-photon sources," Nat. Nanotechnol. **12**, 1026–1039 (2017).
14. Y.-M. He, Y. He, Y.-J. Wei, D. Wu, M. Atatüre, C. Schneider, S. Höfling, M. Kamp, C.-Y. Lu, and J.-W. Pan, "On-demand semiconductor single-photon source with near-unity indistinguishability," Nat. Nanotechnol. **8**, 213–217 (2013).
15. A. V. Kuhlmann, J. H. Prechtel, J. Houel, A. Ludwig, D. Reuter, A. D. Wieck, and R. J. Warburton, "Transform-limited single photons from a single quantum dot," Nat. Commun. **6**, 8204 (2015).
16. N. Somaschi, V. Giesz, L. De Santis, J. C. Loredo, M. P. Almeida, G. Hornecker, S. L. Portalupi, T. Grange, C. Antón, J. Demory, C. Gómez, I. Sagnes, N. D. Lanzillotti-Kimura, A. Lemaítre, A. Auffeves, A. G. White, L. Lanco, and P. Senellart, "Near-optimal single-photon sources in the solid state," Nat. Photonics **10**, 340–345 (2016).
17. T. Huber, A. Predojević, D. Föger, G. Solomon, and G. Weihs, "Optimal excitation conditions for indistinguishable photons from quantum dots," New J. Phys. **17**, 123025 (2015).
18. M. Metcalfe, S. M. Carr, A. Muller, G. S. Solomon, and J. Lawall, "Resolved sideband emission of InAs/GaAs quantum dots strained by surface acoustic waves," Phys. Rev. Lett. **105**, 037401 (2010).
19. H. S. Nguyen, G. Sallen, C. Voisin, P. Roussignol, C. Diederichs, and G. Cassabois, "Optically gated resonant emission of single quantum dots," Phys. Rev. Lett. **108**, 057401 (2012).
20. A. Thoma, P. Schnauber, M. Gschrey, M. Seifried, J. Wolters, J.-H. Schulze, A. Strittmatter, S. Rodt, A. Carmele, A. Knorr, T. Heindel, and S. Reitzenstein, "Exploring dephasing of a solid-state quantum emitter via time- and temperature-dependent Hong-Ou-Mandel experiments," Phys. Rev. Lett. **116**, 033601 (2016).
21. J. C. Loredo, N. A. Zakaria, N. Somaschi, C. Anton, L. de Santis, V. Giesz, T. Grange, M. A. Broome, O. Gazzano, G. Coppola, I. Sagnes, A. Lemaitre, A. Auffeves, P. Senellart, M. P. Almeida, and A. G. White, "Scalable performance in solid-state single-photon sources," Optica **3**, 433–440 (2016).
22. H. Wang, Z.-C. Duan, Y.-H. Li, S. Chen, J.-P. Li, Y.-M. He, M.-C. Chen, Y. He, X. Ding, C.-Z. Peng, C. Schneider, M. Kamp, S. Höfling, C.-Y. Lu, and J.-W. Pan, "Near-transform-limited single photons from an efficient solid-state quantum emitter," Phys. Rev. Lett. **116**, 213601 (2016).
23. J. Yin, J.-G. Ren, H. Lu, Y. Cao, H.-L. Yong, Y.-P. Wu, C. Liu, S.-K. Liao, F. Zhou, Y. Jiang, X.-D. Cai, P. Xu, G.-S. Pan, J.-J. Jia, Y.-M. Huang, H. Yin, J.-Y. Wang, Y.-A. Chen, C.-Z. Peng, and J.-W. Pan, "Quantum teleportation and entanglement distribution over 100-kilometre free-space channels," Nature **488**, 185–188 (2012).
24. C. Xiong, X. Zhang, Z. Liu, M. J. Collins, A. Mahendra, L. G. Helt, M. J. Steel, D.-Y. Choi, C. J. Chae, P. H. W. Leong, and B. J. Eggleton, "Active temporal multiplexing of indistinguishable heralded single photons," Nat. Commun. **7**, 10853 (2016).
25. E. Flagg, A. Muller, S. Polyakov, A. Ling, A. Migdall, and G. Solomon, "Interference of single photons from two separate semiconductor quantum dots," Phys. Rev. Lett. **104**, 137401 (2010).
26. R. B. Patel, A. J. Bennett, I. Farrer, C. A. Nicoll, D. A. Ritchie, and A. J. Shields, "Two-photon interference of the emission from electrically tunable remote quantum dots," Nat. Photonics **4**, 632–635 (2010).
27. D. Chen, G. R. Lander, K. S. Krowpman, G. S. Solomon, and E. B. Flagg, "Characterization of the local charge environment of a single quantum dot via resonance fluorescence," Phys. Rev. B **93**, 115307 (2016).
28. H. Benisty, H. De Neve, and C. Weisbuch, "Impact of planar microcavity effects on light extraction-Part I: basic concepts and analytical trends," IEEE J. Quantum Electron. **34**, 1612–1631 (1998).
29. A. Muller, E. B. Flagg, P. Bianucci, X. Y. Wang, D. G. Deppe, W. Ma, J. Zhang, G. J. Salamo, M. Xiao, and C. K. Shih, "Resonance fluorescence from a coherently driven semiconductor quantum dot in a cavity," Phys. Rev. Lett. **99**, 187402 (2007).
30. A. Muller, W. Fang, J. Lawall, and G. S. Solomon, "Emission spectrum of a dressed exciton-biexciton complex in a semiconductor quantum dot," Phys. Rev. Lett. **101**, 027401 (2008).
31. B. Mollow, "Power spectrum of light scattered by two-level systems," Phys. Rev. **188**, 1969–1975 (1969).
32. A. Ulhaq, S. Weiler, C. Roy, S. M. Ulrich, M. Jetter, S. Hughes, and P. Michler, "Detuning-dependent Mollow triplet of a coherently-driven single quantum dot," Opt. Express **21**, 4382–4395 (2013).
33. R. Loudon, *The Quantum Theory of Light* (Oxford Science Publications, 2000).
34. T. Thomay, S. V. Polyakov, O. Gazzano, E. Goldschmidt, V. Loo, and G. S. Solomon, "Simultaneous, full characterization of a single-photon state using semiconductor quantum-dot light," Phys. Rev. X **7**, 041036 (2017).
35. E. B. Flagg, A. Muller, J. W. Robertson, S. Founta, D. G. Deppe, M. Xiao, W. Ma, G. J. Salamo, and C. K. Shih, "Resonantly driven coherent oscillations in a solid-state quantum emitter," Nat. Phys. **5**, 203–207 (2009).
36. J. J. Finley, M. Sabathil, P. Vogl, G. Abstreiter, R. Oulton, A. I. Tartakovskii, D. J. Mowbray, M. S. Skolnick, S. L. Liew, A. G. Cullis, and M. Hopkinson, "Quantum-confined Stark shifts of charged exciton complexes in quantum dots," Phys. Rev. B **70**, 201308 (2004).
37. J. Houel, A. V. Kuhlmann, L. Greuter, F. Xue, M. Poggio, B. D. Gerardot, P. A. Dalgarno, A. Badolato, P. M. Petroff, A. Ludwig, D. Reuter, A. D. Wieck, and R. J. Warburton, "Probing single-charge fluctuations at a GaAs/AlAs interface using laser spectroscopy on a nearby InGaAs quantum dot," Phys. Rev. Lett. **108**, 107401 (2012).
38. X. Ding, Y. He, Z.-C. Duan, N. Gregersen, M.-C. Chen, S. Unsleber, S. Maier, C. Schneider, M. Kamp, S. Höfling, C.-Y. Lu, and J.-W. Pan, "On-demand single photons with high extraction efficiency and near-unity indistinguishability from a resonantly driven quantum dot in a micropillar," Phys. Rev. Lett. **116**, 020401 (2016).
39. A. Reigue, A. Lemaître, C. G. Carbonell, C. Ulysse, K. Merghem, S. Guilet, R. Hostein, and V. Voliotis, "Resonance fluorescence revival in a voltage-controlled semiconductor quantum dot," Appl. Phys. Lett. **112**, 073103 (2018).

40. A. Kurzmann, A. Ludwig, A. D. Wieck, A. Lorke, and M. Geller, "Auger recombination in self-assembled quantum dots: quenching and broadening of the charged exciton transition," Nano Lett. **16**, 3367–3372 (2016).
41. A. Kurzmann, B. Merkel, P. A. Labud, A. Ludwig, A. D. Wieck, A. Lorke, and M. Geller, "Optical blocking of electron tunneling into a single self-assembled quantum dot," Phys. Rev. Lett. **117**, 1–5 (2016).
42. J. L. Bjorkstam, J. Listerud, M. Villa, and C. I. Massara, "Motional narrowing of a Gaussian NMR line," J. Magn. Reson. **65**, 383–394 (1985).
43. A. Berthelot, I. Favero, G. Cassabois, C. Voisin, C. Delalande, P. Roussignol, R. Ferreira, and J. M. Gérard, "Unconventional motional narrowing in the optical spectrum of a semiconductor quantum dot," Nat. Phys. **2**, 759–764 (2006).
44. H. S. Nguyen, G. Sallen, M. Abbarchi, R. Ferreira, C. Voisin, P. Roussignol, G. Cassabois, and C. Diederichs, "Photoneutralization and slow capture of carriers in quantum dots probed by resonant excitation spectroscopy," Phys. Rev. B **87**, 115305 (2013).